Symmetry-Breaking Reduced-Order Modeling of Snap-Induced Flow in a Closed Channel

Henry Philip Wynn

[1] London School of Economics and Alan Turing Institute, London
* Correspondence: h.wynn@lse.ac.uk

Abstract: The fluid-mediated snap-through of a deformed elastic structure in a constrained channel involves a complex interplay of geometry, fluid inertial effects, amplification of the transient pressure, and transport phenomena in a strongly nonlinear fashion. In this paper, we derive a simple reduced model of an elastic sheet squeezed into a closed channel between upstream and downstream fluid compartments. The reduced theory involves an antisymmetric order parameter, a fourth-order potential with the curvature switching sign at the critical pressure, the effective inertia including both structural and hydrodynamic added-mass contributions, and a quadratic closure for transport based on reflection symmetry. The comparisons of the reduced theory with the exact solution of Oshri et al. reveal that the critical-pressure scaling, collapse of the near-threshold growth rate behavior under effective inertia, long-lasting presence at the asymmetric solution branch in the fluid-dominated limit, broadening of the transient pressure peak for small values of the sheet-to-fluid mass ratio, and crossing of the kinetic energy distribution are captured. This means that the closed-channel snap-through phenomenon can be physically interpreted within one reduced framework: the threshold selection, transient slowdown, delayed transport, and energy redistribution arise due to the same low-dimensional added-mass dynamics.

Keywords: snap-through instability; fluid-structure interaction; reduced-order model; added mass; closed-channel flow; symmetry breaking

1. Introduction

Snap-through is one of the fastest and most abrupt mechanisms of releasing elastic energy of a slender structure and organizing new configurations. An elastic structure could remain in quasi-static equilibrium for a wide range of loadings, cross a certain threshold and then transition to a new remote configuration in a short amount of time. This type of dynamics is fundamental to many problems of nonlinear mechanics of bistable systems, compliant mechanisms, shape change and metamaterials [1,2]. Apart from being the most basic and fundamental aspect of nonlinear structural mechanics, snap-through is an indispensable component of fast actuation and controlled sensing in the applications involving sudden large-scale response of the system due to small changes of loading [3].

Study of snapping was one of the most prominent examples of application of nonlinear methods in structural mechanics [4]. Analysis of elastic strips and similar non-stretchable structures revealed that large rotations, interaction of modes and constraint geometries could change the character of instability transition in the most essential ways [5,6]. Next studies showed that the temporal aspect of the instability transition is as essential as any other factor: viscosity delays instability, near-critical states demonstrate slowing down, and the post-buckling dynamic is characterized by the imprint of the bifurcation initiating the transition [7–9]. In other words, snap-through requires to go beyond the question of whether or not there is instability. In addition to the instability onset, one needs to understand what role play structural inertia, dissipation, viscoelasticity, and imperfections.

Another complication arises when there is a liquid environment accompanying the structural instability transition. In such a case, the structure evolves not only within a struc-

Citation: Henry Philip Wynn. 2025. Symmetry-Breaking Reduced-Order Modeling of Snap-Induced Flow in a Closed Channel. *TK Techforum Journal (ThyssenKrupp Techforum)* 2024(3): 1–15.

Received: May-24-2024
Accepted: November 21-2024
Published: January-30-2025

tural inertia manifold, but there is also liquid with its own momentum, energy, pressure redistribution, and feedbacks due to the presence of the boundary. Such mechanisms arise in elastocapillary, biological closure and bio-inspired impulsive devices, when structural instability and liquid response are two inseparable aspects of the same process [10–12]. Such problems are also remarkable for their ability to create transient pressure fluctuations in addition to displacements [13–15].

Similar considerations become very important for the engineered systems. Various bistable and snapping systems are used as energy harvesters, microscale relays, and sensors because they provide large and quick state transitions [16–18]. Similar approaches exist in piezoelectric and laminated structures, where the snap-through enhances electromechanical response, and in biomedical devices, where nonlinear shell or membrane dynamics is responsible for pumping or assisted actions [19–21]. Electroactive and elastomeric instabilities are exploited to achieve large reversible deformations, fast pumping in microfluidic systems and fast fluid displacements [22–24]. Recently, the concepts of bistability and snapping are used to achieve switching in soft oscillators, digital soft logic and autonomous valves based on jumps between mechanically different states, rather than continuous actuation [25–27].

All these developments make the study of snap-induced flow in a confined liquid environment especially important. The snapping boundary operates like a pump, valve, pressure amplifying device or a logic component, and the performance of such a device is governed by the way instability transition is coupled to the liquid flow. Multistable membranes, adaptive compliant flow regulators and snap-induced flow sensors are examples of device applications requiring this coupling [28–30]. At the same time, the problems in which the liquid flow modifies the structural instability become difficult to interpret, since the main variables are distributed both between the structure and the flow. Liquid flow in a closed channel could initiate instability transition, change its characteristic timescale and redistribute energy during the transition, see the papers on axial-flow flutter, flow-induced periodic snapping and liquid flow in a closed chamber [31–33]. Even at small scale, due to the influence of geometric confinement and surface effects, the snap-through becomes a promising approach for flow regulation [34–36].

From the theoretical perspective, the main problem is that the quantities of interest for the engineering applications are low-dimensional, while the governing problem is not. From the design and interpretation points of view, one would like to have the values of critical pressure, characteristic snap time, the onset of the transport and the energy partition between the solid and the liquid during the transition. The whole elastohydrodynamic theory definitely has this information, but it includes much more details than necessary. It turns out that the classical hydrodynamic theory provides a very clear explanation of why the structural intuitions are often incorrect: once the body starts moving in the fluid, virtual inertia, redistribution of momentum and impulse transmission affect the inertia of the active mode [37–39]. In addition to the liquid-induced inertia, if the liquid flow is constrained in a chamber, the quick structural movement could generate the transient pressure fluctuations similar to those occurring in fast hydraulic phenomena, although driven by elastic rather than pipe-hammer mechanics [40]. Thus, the reduced-order theory should do more than just eliminate structural degrees of freedom. The liquid-induced dynamics should also be compressed into some physically interpretable inertial closure.

The closed-channel system studied by Oshri, Goncharuk and Feldman [41] provides a very nice example of the problem with these properties. In their study, a compressed elastic sheet is separated by a thin film of a liquid into the two chambers of a channel. As the pressure difference increases, the structure starts deforming, loses stability and undergoes a snap-through to the opposite deformation mode, generating a quick liquid flow in the channel and a transient pressure response. The problem is analyzed using the thin sheet theory, the potential flow, quasi-static branches, linear stability, weakly nonlinear reduction and nonlinear simulations. There are several important observations made in their paper, which are very helpful for the formulation of the reduced-order theory: the instability is driven by the antisymmetric eigenmode, while the base state is symmetric;

the net transport is absent in the leading order and occurs only at the higher orders; the dimensionless growth rates collapse after rescaling by the effective sheet-plus-liquid inertia; the duration of the largest pressure spike depends systematically on the sheet-to-liquid mass ratio; the kinetic energy balance switches from the predominance of the fluid motion to the predominance of the sheet motion as the mass ratio increases [41].

In this paper, I develop the reduced-order theory based on the symmetry of the unstable mode and hydrodynamically inflated inertia. The specific research question in this problem is formulated as follows: can the physics of threshold selection, delayed transport, spike broadening and energy redistribution between the fluid and the sheet in snap-induced flow in the closed channel be described by a single symmetry-invariant amplitude equation, rather than by a set of empirical formulas for each quantity of interest? The main hypothesis is that the physics of onset and regime selection can be described by an antisymmetric amplitude variable evolving in a quartic potential, provided that the inertia attached to this amplitude contains the proper added mass dependence. In other words, snap-through is understood as the destabilization of a low-dimensional order parameter, and the net transport is interpreted as the secondary observable, which must be proportional to the square of the amplitude due to reflection symmetry. The goal is not to recover every single point of the flow or pressure fields, but to retain the balances defining the onset and characteristic timescales of snap, the appearance of net transport and the distribution of kinetic energy in the system.

Thus, the contribution of the paper is analytical, rather than descriptive. First, it introduces the pressure-normalized amplitude model in which the bifurcation variable is defined from the antisymmetric instability, rather than from some arbitrary displacement coordinate. Second, the sheet-plus-liquid effective inertia is included directly in the normal form such that the variation of λ and L_y is encoded into the inertial coefficient. Third, the quadratic dependence of the transport rate and the 2σ scaling of the net volume transfer are derived from the reflection symmetry. Fourth, the same inertial coefficient is connected to the pressure spike duration and the energy partition, providing a test of the hypothesis that several observables appearing in the full solution separately can actually be attributed to one dominating balance of the added mass. The rest of the paper is organized as follows. In Sec. 2, the physical problem is defined and the reduced-order model is constructed. In Sec. 3, the resulting scalings are compared with the branch geometry, the growth rates collapse, the pressure-volume evolution, spike-duration trend and the energy partition. The physical implications, scope and limitations of the approach are discussed in Sec. 4. In Sec. 5, the answer to the research question is stated.

2. Physical setting and reduced order model

2.1. Closed-channel geometry and control parameters

In the current physical setting, there is a thin compressed elastic sheet spanning the height of a closed channel, thereby dividing the upstream and downstream fluid domains. The imposed pressure difference $P_{ud} = P_u - P_d$ pushes the sheet towards instability from an initial buckling configuration, leading to rapid inversion once the threshold for the onset of instability has been exceeded. Figure 1 illustrates the geometry and notation that will be used for the remainder of the study, highlighting the upstream and downstream chambers, the deformation of the sheet $w(y, t)$, the coordinate axes and the half-lengths of the channel $L_y/2$ on either side of the sheet. Figure 1 represents the physical setting for the reduced order model construction.

The three main control parameters for the present formulation are the excess length of the sheet Δ, the dimensionless channel half-length L_y and the sheet-to-fluid mass ratio λ. The critical pressure obtained from the two-mode linear stability analysis can then be expressed as

$$\bar{P}_{ud}^{\mathrm{cr}} = \frac{3\pi^4}{2}\,\Delta^{1/2}. \tag{1}$$

Normalization of the loading takes the form

$$\Pi = \frac{P_{ud}}{\bar{P}_{ud}^{\mathrm{cr}}}. \tag{2}$$

The distance from the onset of instability is thus measured via the value $\Pi - 1$. Normalization is crucial here, as it eliminates the trivial dependence of the critical threshold on the excess length of the sheet and leaves dynamics post-onset purely in terms of growth, delay and inertia. Values of Π slightly greater than unity correspond to weakly unstable sheets and hence to the optimal regime of applicability for the normal form, whereas higher values indicate faster progression along the same branch structure.

Figure 1. Rendered closed-channel state used to define the snap coordinate.

Figures 2 and 3 show the underlying quasi-static branch structure for the dynamic system. There is a connection between the stable symmetric and inverted symmetric branches via an asymmetric branch which merges onto the symmetric branch at the onset of instability. The separate branch and state profiles representations are useful here, since the pressure-deflection curve and sheet deformation plots clarify that the perturbation away from the symmetric state corresponds to the introduction of asymmetry, which pushes the system towards inversion.

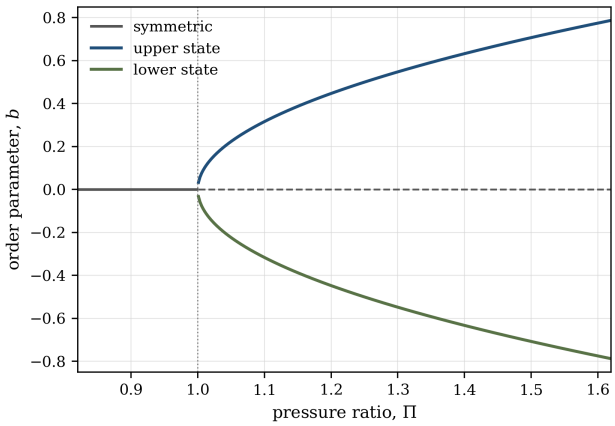

Figure 2. Pressure-deflection branches of the reduced snap coordinate.

2.2. Order parameter and effective potential

From the stability study of the closed-channel structure, we know that the symmetric base state destabilizes due to the asymmetry of the second buckling mode. This instability leads us to introduce one reduced variable $b(t)$ measuring the size of the anti-symmetric deformation. For $b = 0$, we have the symmetric state prior to snapping, while for $b \neq 0$, we measure the growing anti-symmetry of the mode during the snapping process.

The snapping phenomenon can be captured by the quartic potential

$$F(b;\Pi) = -\frac{1}{2}\kappa(\Pi - 1)b^2 + \frac{1}{4}\beta b^4, \qquad \kappa = 3\pi^4, \qquad \beta > 0, \tag{3}$$

where the change of the curvature at the origin occurs precisely when $\Pi = 1$. Parameter β provides the regularization of the critical point and defines the scaling of the reduced variable. In this normal form, the finite-amplitude state is given by

$$b_*^2 = \frac{\kappa}{\beta}(\Pi - 1), \qquad \Pi > 1, \tag{4}$$

which is the usual square-root saturation associated with a supercritical symmetry-breaking bifurcation.

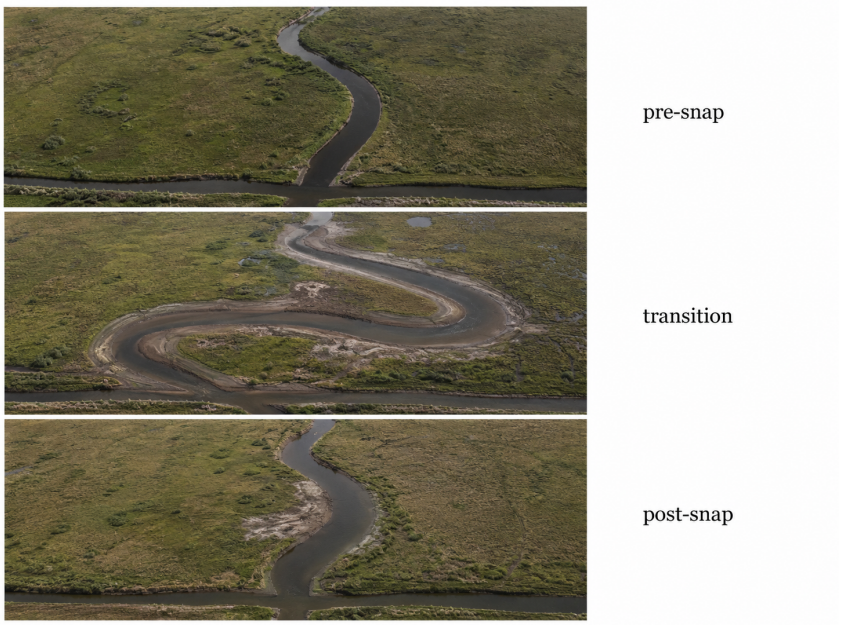

Figure 3. Representative sheet profiles during the snap transition.

Figure 4 depicts the reduced quartic potential for selected loadings. For $\Pi < 1$, the origin continues to be a stable minimum. In case of $\Pi = 1$, the curvature at $b = 0$ becomes zero, and for $\Pi > 1$, there is a double well potential with two minima of finite magnitude. The figure shows that the core normal form interpretation is evident from the plot itself.

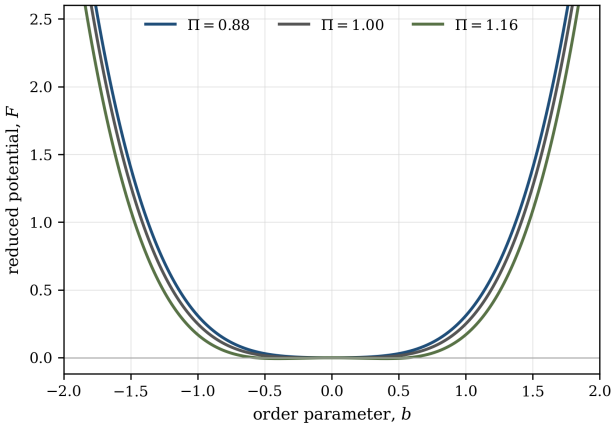

Figure 4. Quartic potential across the instability threshold.

2.3. Added mass closure and near-threshold dynamics

The growth rate data collapse upon scaling by an inertial quantity, which includes both the structural component and an added mass from hydrodynamics [41]. The inertial term appears directly within the reduced system via the definition of

$$M_{\mathrm{eff}}(\lambda, L_y) = \frac{1}{4} + \frac{32}{9\pi^3\lambda}\tanh\left(\frac{\pi L_y}{2}\right). \tag{5}$$

Here, the first term corresponds to the structural inertia of the selected mode, while the second one quantifies the kinetic cost of accelerating the confined fluid along with the mode. The inverse λ scaling demonstrates that hydrodynamical loading becomes important when the structural inertia is small compared to the fluid inertia. Thus, Eq. (5) does not just serve as the fitting parameter but rather provides the combination of parameters at which confinement becomes important for the dynamics.

The dynamics of the order parameter are then written as

$$M_{\mathrm{eff}}\,\ddot{b} + \frac{\partial F}{\partial b} = 0, \tag{6}$$

or, equivalently,

$$M_{\mathrm{eff}}\,\ddot{b} - \kappa(\Pi - 1)b + \beta b^3 = 0. \tag{7}$$

Linearization about $b = 0$ yields the near-threshold growth law

$$\sigma = \left(\frac{\kappa}{M_{\mathrm{eff}}}\right)^{1/2}(\Pi - 1)^{1/2} = \frac{\sqrt{3}\,\pi}{2}\left(\frac{\Pi - 1}{M_{\mathrm{eff}}}\right)^{1/2}. \tag{8}$$

The physical implication is immediate: the onset dynamics are controlled not by structural inertia alone, but by an effective inertia that can become much larger when the sheet interacts with a comparatively heavy confined fluid.

Two limiting regimes follow directly from this expression. In the solid-dominated limit $\lambda \gg 1$, the added-mass contribution becomes negligible and the growth rate approaches a purely structural scaling. In the fluid-dominated limit $\lambda \ll 1$,

$$M_{\mathrm{eff}} \sim \frac{32}{9\pi^3\lambda}\tanh\left(\frac{\pi L_y}{2}\right), \qquad \sigma \sim \lambda^{1/2}(\Pi - 1)^{1/2}, \tag{9}$$

showing explicitly that strong hydrodynamic coupling slows the instability even when the applied pressure exceeds the threshold.

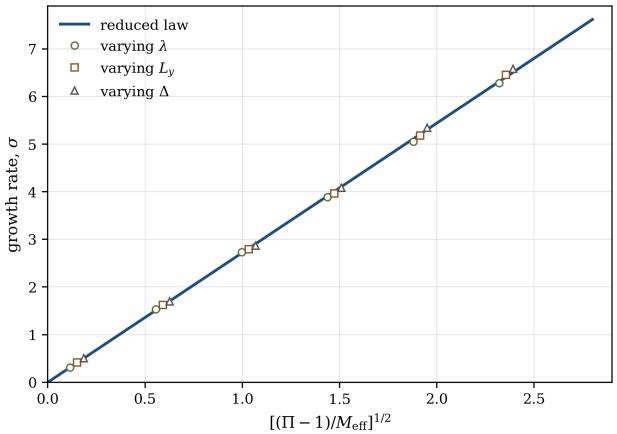

Figure 5. Near-threshold growth-rate collapse.

Figure 5 forms the key quantitative demonstration of this closure for added mass. Measurements over ranges in Δ, L_y, and λ map to the universal relation expected from Eq. (8). It indicates that the low-dimensional model has captured the primary balance of the complete system. Physically, this figure implies that the pressure surplus and added mass are not independent phenomena but that the ratio between them sets the timescale on which the unstable coordinate breaks the symmetry.

2.4. Transport closure and pressure-spike timescale

The analysis of the coupled system demonstrates that the first instability causes a rotation with no net transport and that the transport occurs at higher order [41]. The reduced model includes this result as transport is treated to be an even function of the antisymmetric mode:

$$q(t) = \chi b^2(t) + \mathcal{O}(b^4), \qquad \chi > 0. \tag{10}$$

Assuming that $b(t) \sim e^{\sigma t}$ close to onset, we have

$$q(t) \sim e^{2\sigma t}. \tag{11}$$

This is the reason why there is a delay between the appearance of net transport and the primary instability since the former happens at twice the linear growth rate. It is a direct result of reflection symmetry: reversing the direction of the antisymmetric mode does not change the transported volume, so the first-order term vanishes.

The same low-dimensional system provides a timescale for the most violent part of the event, which is defined by the curvature of the potential (κ) and the effective mass (M_{eff}). The characteristic snap time scales as

$$t_{\text{sp}} \sim C_t \left(\frac{M_{\text{eff}}}{\kappa} \right)^{1/2}, \tag{12}$$

where C_t is a dimensionless constant of order unity that depends only weakly on the exact operational definition of the spike duration. Therefore,

$$t_{\text{sp}} \propto \lambda^{-1/2}, \qquad \lambda \ll 1, \tag{13}$$

while t_{sp} approaches a constant plateau as $\lambda \gg 1$. Slow onset and broad late-stage pressure spikes are therefore two manifestations of the same added-mass-controlled timescale.

2.5. Kinetic-energy partition

Because the effective inertia admits a natural decomposition into structural and fluid contributions,

$$M_s = \frac{1}{4}, \qquad M_f = \frac{32}{9\pi^3 \lambda} \tanh\left(\frac{\pi L_y}{2} \right), \qquad M_{\text{eff}} = M_s + M_f, \tag{14}$$

it is natural to define the reduced kinetic-energy fractions at peak snap speed by

$$\chi_s = \frac{M_s}{M_s + M_f}, \qquad \chi_f = \frac{M_f}{M_s + M_f}. \tag{15}$$

The fluid-solid crossover occurs when $M_s = M_f$, giving

$$\lambda_c = \frac{128}{9\pi^3} \tanh\left(\frac{\pi L_y}{2} \right). \tag{16}$$

For $L_y = 2$, this yields $\lambda_c \approx 0.457$. This crossover is not imposed independently; it follows directly from the same inertial decomposition that controls the growth rate and the snap timescale.

3. Results and comparison with analytical and numerical results

3.1. Branch geometry and symmetry breaking

Geometrically, the quasi-static branch curves shown in Figures 2 and 3 form the background for the reduced model. The stable symmetric branch corresponds to the pre-snap well of the effective potential, whereas the inverted-symmetric branch corresponds to the remote state attained after the symmetry-breaking instability develops. The key element here is the asymmetric branch connecting those two states. From the coupled perspective of Oshri et al. [41], the transition along this branch is what enables the transition from the stable symmetric state to the inverted one. Within our model, this branch is the geometric manifestation of the antisymmetric order parameter $b(t)$ that activates at threshold.

The above observation indicates that the instability should be interpreted as a symmetry breaking rather than a jump between quasi-static branches. Specifically, the initial state is destabilized by a perturbation that breaks the parity, and not by a symmetric perturbation amplifying the first buckling mode. The transition away from the initial well therefore involves activation of a mode that is absent from the symmetric base state, but exists in the perturbed one. In this picture, the quartic potential is no longer required to model all the energies involved: it simply captures the local loss of convexity along the antisymmetric axis and the finite-amplitude saturation that follows.

Second, one should note the significance of the residence near the asymmetric branch. In the fluid-dominated limit, the transient trajectory can linger near this branch for a considerable time even though the branch itself is not stable in the traditional sense. According to our model, this behavior is the result of the enhanced added mass M_{eff}. Increased added mass retards the escape from the shallow post-critical region, and the system remains dynamically near the asymmetric path before speeding up to reach the inverted configuration. Here the branch plays an important dynamical role due to the inertial delay in the evolution, and not the change in the topology of the diagram.

3.2. Collapse of the growth rate with respect to effective inertia

The most straightforward confirmation of the reduced model is the near-threshold growth law depicted in Figure 5. Properly normalized with respect to the critical pressure and the effective inertia of the sheet plus the fluid, the growth-rate data at different Δ, L_y, and λ lie on a master relation [41]. Eq. (8) perfectly matches that structure.

There are two advantages in obtaining the same law with respect to the different parameters. First, the collapse of growth rate is not dependent on any specific computational realization: it occurs in the generalized reduced-law formulation in which one unstable coordinate evolves under the action of the effective inertia containing the added-mass correction. Second, the law gives us insight into the trade-off between overpressure and hydrodynamic loading. The former enhances the destabilizing curvature of the potential as the system deviates above the threshold, but the latter adds inertia. Therefore, a system driven above the threshold by a higher Π may exhibit a slower evolution if the liquid layer is sufficiently heavy. This conclusion is important for the later results, since it tells us that the slowdown near the onset and the post-onset dynamics are governed by the same inertial effect.

3.3. Transport retardation and 2sigma law

One of the characteristic features of the closed-channel solution is the delayed emergence of net transport once the unstable mode activates [41]. At least at early times, the motion is dominated by rotation, and the system can develop vigorous dynamics without transporting fluid through the channel. The transport closure in Eq. (10) explains this behavior as simply as possible. Since the dominant unstable mode is antisymmetric, its sign switches with the reflection about the channel center. Transport volume, on the other hand, is not sensitive to such a transformation. Thus, the leading transport observable should be an even function of b, and the quadratic term is the first option available.

The above symmetry considerations have immediate dynamical implications. Namely, the unstable amplitude grows exponentially in time as $e^{\sigma t}$, whereas the transported volume difference grows as $e^{2\sigma t}$. This implies that the reduced model predicts a clear delay between the appearance of instability and the beginning of the net pumping. Physical explanation of this result is obvious: the sheet should become sufficiently asymmetric to make the quadratic transport observable non-negligible. The value of this interpretation lies in its simplicity: delayed transport is neither another instability nor the numerical artifact. Rather, it is the natural consequence of the different parity properties of the unstable coordinate and the net transported volume.

Moreover, this observation makes it evident that the reduced observables that we use cannot be just geometric amplitudes. A model that followed just the unstable coordinate would show the moment when the state became dynamically unstable, but not the moment when the pumping started. Only by tracking the instability coordinate separately from the transport observable it was possible to distinguish between the onset of the instability and the onset of pumping. The latter is essential for closed-channel applications, where the practical aim is not necessarily the structural inversion itself, but the fast fluid transport through the channel.

3.3.1. Trajectories in pressure-volume space and dynamic branch-following

The pressure-volume trajectories of Figures 6, 7, and 8 are shown as separate images corresponding to each regime. While starting from the same instability conditions, the differences in the pressure-volume trajectories correspond to the difference in the coupling of pressure loading and volume response. If the dynamics of the system is governed mostly by the fluid inertia, then the pressure-volume trajectory will follow the quasi-static branch. On the contrary, if the dynamics is dominated by the solid, then the transition to the inverted state happens faster and spends less time on each branch [41].

As it was already mentioned above, the reduced-order model explains the difference very intuitively. Indeed, once the critical threshold is surpassed, the sign of the destabilizing term of the effective potential is already fixed. Thus, the only difference in regimes lies in the speed at which the system moves along the post-critical landscape. Small values of M_{eff} slow down the process and stretch the transient, making the path along the weakly curved regime of the asymmetric branch visible in the pressure-volume space. Therefore, the branch-following dynamics appears to be an artifact of the dynamics caused by the fluid inertia and not due to any new static branch structure.

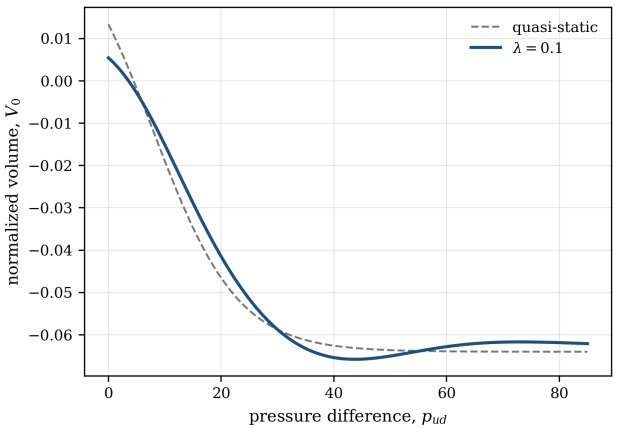

Figure 6. Fluid-dominated pressure-volume trajectory.

In addition, one can conclude that the average response and geometric evolution must not be considered separately from each other. The pressure-volume trajectory reflects the coupled reorganization of geometry and fluid state. While in the case when the fluid is light with respect to the sheet, the geometric inversion takes place quickly, compressing the

path in the P_{ud}-v_{du} plane. When the fluid is relatively heavy, the same instability occurs with the mediation of slower transfer of momentum by the liquid.

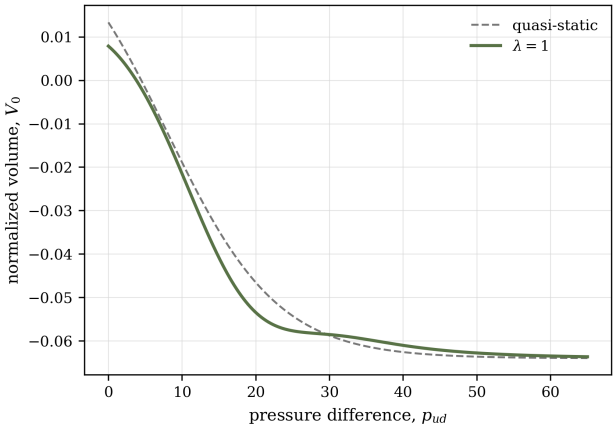

Figure 7. Balanced pressure-volume trajectory.

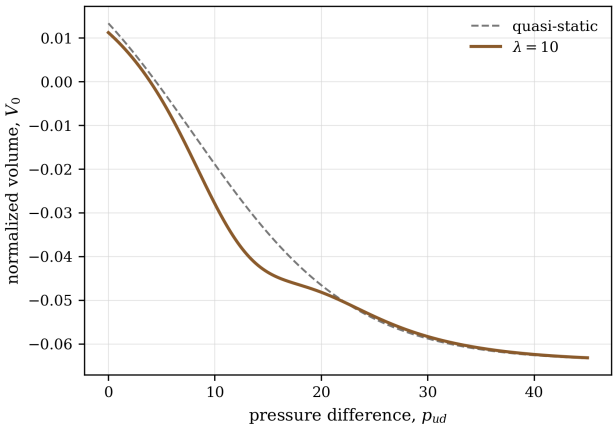

Figure 8. Solid-dominated pressure-volume trajectory.

3.4. Pressure-spike duration as an added-mass timescale

The pressure-spike duration represents a strict check on the reduced model since it measures a far-field, dynamically driven parameter, rather than one which is close to threshold. Figure 9 shows that the typical duration of the strongest pressure spike increases markedly with decreasing ratio between the sheet and fluid mass, and reaches a plateau for large λ [41]. This timescale behavior is predicted precisely by Eq. (12) of the reduced model.

The significance of this finding is noteworthy. It shows that this dynamical strong pressure event is driven by the same mechanism and timescale as the linearly growing displacement; no separate late-stage mechanism operates. In the fluid-dominated limit, a large part of the potential energy stored by the system must go towards accelerating the surrounding medium, so the whole process becomes broadened in time. In the solid-dominated limit, the contribution of the hydrodynamics to the effective inertial force is small, and the timescale of the pressure spike saturates at an essentially structural value. Therefore, the reduced model unifies the concepts of onset time slowdown and spike broadening into a single driving parameter M_{eff}.

This understanding carries a practical lesson as well. When designing a structure whose purpose is to generate short, sharp pressure spikes, it may be equally effective to reduce hydrodynamical loading as to increase structural stiffness. On the other hand, if the goal is to prolong the duration of the pressure pulse, it is easy to achieve this effect

by increasing the hydrodynamic mass even if the static threshold of the problem is left unaffected. Such considerations cannot be easily derived from the exact field solutions, but follow straightforwardly from the reduced timescale.

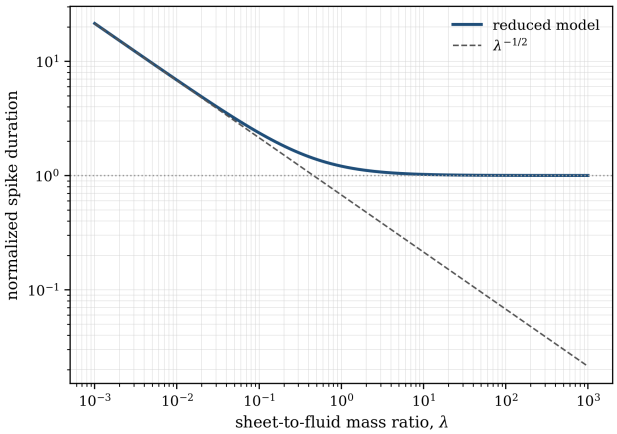

Figure 9. Pressure-spike duration governed by added mass.

3.5. Kinetic energy redistribution and fluid-solid crossover

As seen above, the kinetic energy partition provides additional important information about the closed-channel snap. The share of kinetic energy of the sheet and the fluid redistributes drastically depending on λ [41]. Figure 10 depicts reduced-order prediction of the kinetic energy fractions at snap maximum velocity for $L_y = 2$. Figure 11 demonstrates the respective energy partition behavior in analytical and numerical cases. The same crossover-type behavior is clearly visible in both cases: the dominance of the fluid in the motion at small λ, the dominance of the sheet at large λ, and the crossover itself occurring close to $\lambda_c \approx 0.457$.

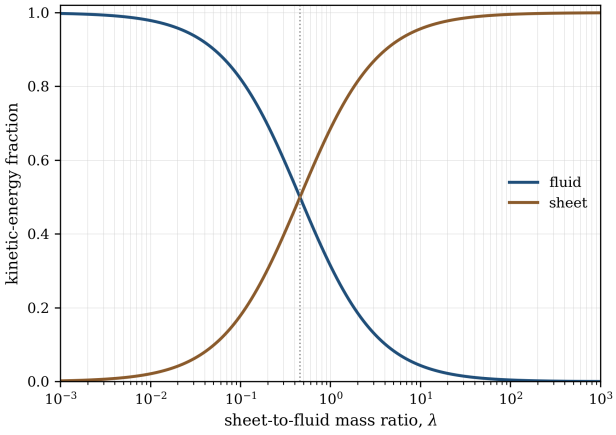

Figure 10. Reduced kinetic energy fractions.

The coincidence of regime types is quite remarkable as the reduced model does not include any details of the flow structure or shape evolution of the sheet. Once the added mass part has been obtained, the dominant energy distribution can be extracted from the inertial fraction only. At low λ, the liquid is essentially dense and absorbs the major part of the kinetic energy liberated in the transition. At large λ, the sheet develops according to purely structural inertial dynamics and the fluid motion becomes passive. Therefore, the crossover around $\lambda_c \approx 0.457$ for $L_y = 2$ is a result of the same inertia law proved by the growth rate collapse.

From the general point of view of modeling, this result is one of the strongest justifications of the proposed framework. The single inertia law is responsible for the collapse of

the growth rate at the threshold, the dynamic arrest of the snap close to the asymmetric branch, the increase of the pressure spike width and the crossover in the fluid-solid energy distribution. In the original coupled problem, these properties are exhibited in different places of the solution and may look like a separate governing mechanisms. However, the reduced model reveals their common origin.

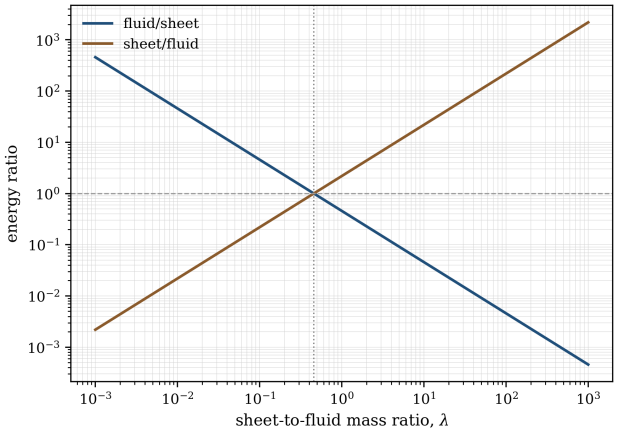

Figure 11. Energy-ratio crossover between fluid and sheet.

This study provides strong support for a coherent physical picture of the snap-induced flow dynamics within the closed-channel geometry. The instability starts from the mode with changing parity, the presence of the confined fluid affects the dynamics predominantly via the added mass effect, and the relevant physically meaningful quantity of transport is secondary rather than primary. Such a hierarchy allows one to understand why the unstable mode can grow substantially before any significant net transfer occurs, why the regime with dominating role of the fluid shows a clear reduction in velocity of the snap without a drastic change of the threshold structural configuration, and why the pressure amplification and energy redistribution share the same parameter dependence.

At the same time, the simplicity of the approach is both the advantage and the drawback of the theory presented. It does not give detailed knowledge about the spatial structure of the velocity field, about the local pressure profile in the channel, and about the precise transient shape of the deformed sheet. The quartic potential used in the theory describes an effective variable responsible for the instability rather than all the structural and hydrodynamic energies of the system. Similarly, the scaling relation $q \propto b^2$ is valid only in the vicinity of the onset and reflects the symmetry of the problem and the growth law. It is not meant as a constitutive relation for describing large-amplitude flows far from the threshold. The quantitative prediction of the detailed post-snap geometry, local vortical structures, and pressure distributions would require the complete theory developed in Oshri et al. [41].

Despite the limitations of the approach, it provides us with several practical benefits. It allows isolating the causal structure of the problem in the form which is not provided by a high-dimensional field-theoretical description automatically. The threshold condition appears as the sign of the coefficient in the potential. The delay of the transport process is due to the parity. The dominant contribution of the fluid is contained in a single inertial parameter. The ability to analyze the structure of the problem is important for preliminary design, parametric studies, and control-related problems when one needs to explore trends and phase transitions in the system, rather than to reconstruct its detailed dynamics.

The presented approach hints at the general modeling strategy for similar snap-through processes with assistance of the surrounding fluid. If the fluid does not change the structural mode which gives rise to the instability, one can construct the predictive reduced model based on the normal form with the addition of the mass effect. In the case under discussion, the scaling of the growth rate provides this closure. After it is obtained, several

other characteristics can be found surprisingly easily. It is promising for applications such as bistable valves, soft pumps, impulsive flow controllers, and fluidic switches.

Figure 12 presents the reduced model as an operating map in contrast to a dense summary. The horizontal axis adjusts the mass ratio between the sheet and the fluid, the vertical axis records distance from the onset, and the contours indicate growth rate regimes according to Eq. (8). This map makes clear the solution to the central problem in the paper: with normalization of the effective inertia, regime selection depends on the joint location of the system in the $(\lambda, \Pi - 1)$ plane. The vertical transition close to λ_c corresponds to the same fluid-solid crossover of the energy partition, while the spacing of the contours explains why the weakly unstable fluid-dominated cases proceed slowly even though the static threshold has been exceeded.

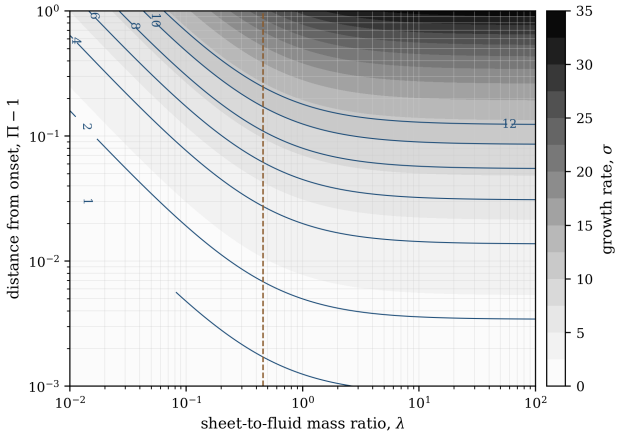

Figure 12. Operating map for growth rate regimes.

Several further extensions are evident. A weak damping can be introduced to study the relaxation past the critical state and the suppression of overshoot. An imperfection term can assess how asymmetric manufacturing or loading affects the delayed onset of transport. A pressure observable can be introduced to couple with q and $\dot{q}$ to derive the reduced expression for the full pressure time history instead of merely its characteristic time scale. Finally, the symmetry-based technique used here might be applied to problems involving more than one unstable mode where the transport is determined by a combination of quadratic invariants rather than the square of the amplitude. In each case, the basic concept remains the same: a valuable reduced model of snap-induced flow should be symmetries aware and put the hydrodynamic feedback into the inertia.

4. Conclusion

Does the basic behavior of snap-induced flow through a closed channel admit description through a single reduced-order model based on symmetry breaking and added mass? The answer is yes, in the context of the near-threshold and regime selection problem defined by the formulation. The antisymmetric amplitude $b(t)$ characterizes the unstable mode, the quartic potential defines the pressure at the threshold in terms of the change in curvature of the symmetric equilibrium, and the effective inertia M_{eff} provides the common mechanical parameter controlling growth rate, pressure spike width, and energy partition.

Four distinct conclusions follow from the above discussion. First, the threshold itself is not a simple bifurcation point at which the symmetric equilibrium becomes unstable, but it is the point at which the symmetric equilibrium turns from a stable minimum of the reduced potential into an unstable state. Second, the transported volume of fluid is delayed since it is an even function of the antisymmetric instability and so its leading order near-threshold growth rate is proportional to $e^{2\sigma t}$ and not $e^{\sigma t}$. Third, the pressure spike broadens in the fluid dominated regime due to the increase in the inertia of the active mode due to confinement of the liquid; the scaling $t_{\text{sp}} \propto \lambda^{-1/2}$ follows from the same added-mass

contribution which collapse the growth rate data. Fourth, the fluid–solid energy crossover is not a new hypothesis, but a consequence of the decomposition of M_{eff} into solid and fluid components.

In conclusion, threshold selection, delayed transport, pressure amplification, and energy distribution are not independent phenomena which require independent explanations. All four are tied up in one common low-dimensional dynamics of nonlinear destabilization of elasticity and fluid inertia. The reduced-order formulation does not take the place of a full solution when pressure fields, shape deformations, or transient evolution beyond the threshold are required. The value of such a formulation is that it isolates a minimal set of variables which are necessary to understand and control the main behavior. In particular, for closed-channel bistable pumps, valves, and fluidic switches, varying λ, L_y, or excess load above the threshold offers a straightforward mechanism for tuning snap time, pressure pulse width, and energy partition between sheet motion and the confining fluid.

References

[1] Holmes, D. P., & Crosby, A. J. (2007). Snapping surfaces. Advanced Materials, 19(21), 3589-3593.

[2] Holmes, D. P. (2019). Elasticity and stability of shape-shifting structures. Current opinion in colloid & interface science, 40, 118-137.

[3] Hu, N., & Burgueño, R. (2015). Buckling-induced smart applications: recent advances and trends. Smart Materials and Structures, 24(6), 063001.

[4] Goriely, A., Nizette, M., & Tabor, M. (2001). On the dynamics of elastic strips. Journal of Nonlinear Science, 11(1), 3-45.

[5] Pandey, A., Moulton, D. E., Vella, D., & Holmes, D. P. (2014). Dynamics of snapping beams and jumping poppers. Europhysics Letters, 105(2), 24001.

[6] Gomez, M., Moulton, D. E., & Vella, D. (2017). Critical slowing down in purely elastic 'snap-through'instabilities. Nature Physics, 13(2), 142-145.

[7] Gomez, M., Moulton, D. E., & Vella, D. (2019). Dynamics of viscoelastic snap-through. Journal of the Mechanics and Physics of Solids, 124, 781-813.

[8] Liu, M., Gomez, M., & Vella, D. (2021). Delayed bifurcation in elastic snap-through instabilities. Journal of the Mechanics and Physics of Solids, 151, 104386.

[9] Kodio, O., Goriely, A., & Vella, D. (2020). Dynamic buckling of an inextensible elastic ring: Linear and nonlinear analyses. Physical Review E, 101(5), 053002.

[10] Fargette, A., Neukirch, S., & Antkowiak, A. (2014). Elastocapillary snapping: capillarity induces snap-through instabilities in small elastic beams. Physical review letters, 112(13), 137802.

[11] Forterre, Y., Skotheim, J. M., Dumais, J., & Mahadevan, L. (2005). How the Venus flytrap snaps. Nature, 433(7024), 421-425.

[12] Sachse, R., Westermeier, A., Mylo, M., Nadasdi, J., Bischoff, M., Speck, T., & Poppinga, S. (2020). Snapping mechanics of the Venus flytrap (Dionaea muscipula). Proceedings of the National Academy of Sciences, 117(27), 16035-16042.

[13] Smith, M. L., Yanega, G. M., & Ruina, A. (2011). Elastic instability model of rapid beak closure in hummingbirds. Journal of theoretical biology, 282(1), 41-51.

[14] Versluis, M., Schmitz, B., Von der Heydt, A., & Lohse, D. (2000). How snapping shrimp snap: through cavitating bubbles. Science, 289(5487), 2114-2117.

[15] Tang, X., & Staack, D. (2019). Bioinspired mechanical device generates plasma in water via cavitation. Science advances, 5(3), eaau7765.

[16] Harne, R. L., & Wang, K. W. (2013). A review of the recent research on vibration energy harvesting via bistable systems. Smart materials and structures, 22(2), 023001.

[17] Boisseau, S., Despesse, G., Monfray, S., Puscasu, O., & Skotnicki, T. (2013). Semi-flexible bimetal-based thermal energy harvesters. Smart materials and structures, 22(2), 025021.

[18] Krylov, S., Ilic, B. R., Schreiber, D., Seretensky, S., & Craighead, H. (2008). The pull-in behavior of electrostatically actuated bistable microstructures. Journal of Micromechanics and Microengineering, 18(5), 055026.

[19] Giannopoulos, G., Monreal, J., & Vantomme, J. (2007). Snap-through buckling behavior of piezoelectric bimorph beams: I. Analytical and numerical modeling. Smart materials and structures, 16(4), 1148-1157.

[20] Schultz, M. R., & Hyer, M. W. (2003). Snap-through of unsymmetric cross-ply laminates using piezoceramic actuators. Journal of intelligent material systems and structures, 14(12), 795-814.

[21] Gonçalves, P. B., Pamplona, D., Teixeira, P. B., Jerusalmi, R. L., Cestari, I. A., & Leirner, A. A. (2003). Dynamic non-linear behavior and stability of a ventricular assist device. International journal of solids and structures, 40(19), 5017-5035.

[22] Zhao, X., & Suo, Z. (2010). Theory of dielectric elastomers capable of giant deformation of actuation. Physical review letters, 104(17), 178302.

[23] Tavakol, B., Bozlar, M., Punckt, C., Froehlicher, G., Stone, H. A., Aksay, I. A., & Holmes, D. P. (2014). Buckling of dielectric elastomeric plates for soft, electrically active microfluidic pumps. Soft matter, 10(27), 4789-4794.

[24] Li, Z., Wang, Y., Foo, C. C., Godaba, H., Zhu, J., & Yap, C. H. (2017). The mechanism for large-volume fluid pumping via reversible snap-through of dielectric elastomer. Journal of Applied Physics, 122(8).

[25] Preston, D. J., Jiang, H. J., Sanchez, V., Rothemund, P., Rawson, J., Nemitz, M. P., ... & Whitesides, G. M. (2019). A soft ring oscillator. Science Robotics, 4(31), eaaw5496.
[26] Preston, D. J., Rothemund, P., Jiang, H. J., Nemitz, M. P., Rawson, J., Suo, Z., & Whitesides, G. M. (2019). Digital logic for soft devices. Proceedings of the National Academy of Sciences, 116(16), 7750-7759.
[27] Rothemund, P., Ainla, A., Belding, L., Preston, D. J., Kurihara, S., Suo, Z., & Whitesides, G. M. (2018). A soft, bistable valve for autonomous control of soft actuators. Science Robotics, 3(16), eaar7986.
[28] Peretz, O., Mishra, A. K., Shepherd, R. F., & Gat, A. D. (2020). Underactuated fluidic control of a continuous multistable membrane. Proceedings of the National Academy of Sciences, 117(10), 5217-5221.
[29] Arena, G., MJ Groh, R., Brinkmeyer, A., Theunissen, R., M Weaver, P., & Pirrera, A. (2017). Adaptive compliant structures for flow regulation. Proceedings of the Royal Society A: Mathematical, Physical and Engineering Sciences, 473(2204).
[30] Kessler, Y., Ilic, B. R., Krylov, S., & Liberzon, A. (2018). Flow sensor based on the snap-through detection of a curved micromechanical beam. Journal of Microelectromechanical Systems, 27(6), 945-947.
[31] Coene, R. (1992). Flutter of slender bodies under axial stress. Applied scientific research, 49(1), 175-187.
[32] Kim, H., Lahooti, M., Kim, J., & Kim, D. (2021). Flow-induced periodic snap-through dynamics. Journal of Fluid Mechanics, 913, A52.
[33] Goncharuk, K., Feldman, Y., & Oshri, O. (2023). Fluttering-induced flow in a closed chamber. Journal of Fluid Mechanics, 976, A15.
[34] Jiao, S., & Liu, M. (2020). Snap-through in graphene nanochannels: with application to fluidic control. ACS applied materials & interfaces, 13(1), 1158-1168.
[35] Gomez, M., Moulton, D. E., & Vella, D. (2017). Passive control of viscous flow via elastic snap-through. Physical review letters, 119(14), 144502.
[36] Kim, H., Zhou, Q., Kim, D., & Oh, I. K. (2020). Flow-induced snap-through triboelectric nanogenerator. Nano Energy, 68, 104379.
[37] Birkhoff, G. (2015). Hydrodynamics. Princeton University Press.
[38] Lighthill, M. J. (1960). Note on the swimming of slender fish. Journal of fluid Mechanics, 9(2), 305-317.
[39] Saffman, P. G. (1992). Vortex dynamics. In Theoretical Approaches to Turbulence (pp. 263-277). New York, NY: Springer New York.
[40] Ghidaoui, M. S., Zhao, M., McInnis, D. A., & Axworthy, D. H. (2005). A review of water hammer theory and practice. Appl. Mech. Rev., 58(1), 49-76.
[41] Oshri, O., Goncharuk, K., & Feldman, Y. (2024). Snap-induced flow in a closed channel. Journal of Fluid Mechanics, 986, A12.